Am J Transl Res 2022;14(11):7782-7791
www.ajtr.org /ISSN:1943-8141/AJTR0146087

Original Article

Value of three-dimensional volume contrast imaging C combined with magnetic resonance imaging for diagnosis of fetal cerebellar vermis and posterior cranial fossa

Xiaojun Ding[1], Zhiping Huang[1], Xiaoyu Liu[2], Lin Lin[1], Min Liu[1], Jie Yang[1], Huan Lu[3]

Departments of [1]Ultrasound Medicine, [2]Medical Imaging, Ganzhou People's Hospital, Ganzhou 341000, Jiangxi, China; [3]Department of Ultrasound Medicine, The First Affiliated Hospital of Gannan Medical University, Ganzhou 341000, Jiangxi, China

Received August 22, 2022; Accepted October 26, 2022; Epub November 15, 2022; Published November 30, 2022

Abstract: Objective: To assess the value of three-dimensional volume contrast imaging C (VCI-C) combined with magnetic resonance imaging (MRI) in the diagnosis of fetal posterior cranial cavity disease. Methods: This study retrospectively analyzed the imaging data of 100 pregnant women with diagnosed abnormal development of fetal cerebellar vermis or posterior cranial fossa in our hospital from January 2020 to February 2022. VCI-C combined with MRI was used to evaluate the morphology of fetal cerebellar vermis, and the display of primary fissures and secondary fissures. The angle between the brain stem and cerebellar vermis (BVA) and the angle between brain stem and cerebellar tentorium (BTA) were measured and compared through MRI images. Results: There was no significant difference between VCI-C and MRI in measuring the height, anteroposterior diameter, or area, BVA and BTA of fetal cerebellar vermis in the normal control group (P > 0.05). It can be considered that the two imaging methods are consistent in measuring the height, anteroposterior diameter and area, BVA, and BTA of the fetal cerebellar vermis in the normal control group. There was no significant difference between VCI-C and MRI in measuring the height, anterior posterior diameter and area, BVA, or BTA of the vermis in the group of fetal cerebellar vermis dysplasia (P > 0.05). The two imaging methods were comparable for all these measurements. Conclusion: Combining three-dimensional VCI-Cwith MRI diagnosis, the median sagittal section of the cerebellar vermis can be observed, the morphologic structure of the vermis, and the anatomical structure of the posterior cranial fossa can be reflected stereoscopically. Quantitative indexes can be measured and calculated to evaluate the developmental abnormalities of the fetal cerebellar vermis and the lesions of the posterior cranial fossa. Their combined effect is better than that of a single application.

Keywords: Three-dimensional VCI-C, MRI, fetal posterior cranial cavity disease, diagnosis

Introduction

The identification and observation of fetal posterior cranial cavity disease is an important part of prenatal ultrasound diagnosis of fetal central nervous system development [1]. It is of great significance to find abnormalities in the nervous system. In particular, the abnormal development of cerebellar vermis is closely related to various malformation syndromes. The prognosis of various malformations in the posterior cranial fossa of the fetus varies greatly, from normal variation to severe craniocerebral malformation [2, 3]. Therefore, prenatal diagnosis and differential diagnosis of these diseases are helpful to evaluate the prognosis of the disease and to decide whether to terminate pregnancy. Assessing the location of the sinus sink and the integrity of the cerebellar vermis is helpful for the accurate and differential diagnosis of posterior fossa malformation [4]. The sinus confluence is easily affected by the acoustic shadow of the fetal skull and is difficult to clearly display on ultrasound image [5]. However, the position of the sinus confluence can be indirectly evaluated by observing the shape of the tentorium cerebelli.

In 2012, the position of the cerebellar tentorium in mid-pregnancy was quantitatively assessed in a study that measured the angle between brain stem and cerebellar vermis (BVA) and the angle between brain stem and cerebellar tentorium (BTA) [6]. Due to the small size, irregular shape, and complex adjacent tissue structure of fetal cerebellum, accurate evaluation of fetal cerebellar development is a difficulty of prenatal ultrasound. The cerebellar vermis is a narrow longitudinal part located between the bilateral cerebellar hemispheres [7]. Its shape is similar to a flat kidney. On sagittal section of the fetal cerebellar vermis, it has a shape of orange petals. The integrity of the cerebellar vermis can be judged by morphologic observation (orange petals, primary fissure, and secondary fissure) [8]. In recent years, three-dimensional ultrasound has provided a new method for observing sagittal sections of the fetal cerebellar vermis, which has improved the diagnosis of posterior fossa malformation to an accuracy of 90% [9]. The three-dimensional volume contrast imaging C (VCI-C) scans the whole cerebellum through the angle with the minimum attenuation of fetal bones [10]. After obtaining the three-dimensional volume data, the standard midsagittal section of the cerebellar vermis is obtained by adjusting the X, Y, and Z axes representing three orthogonal sections, thus overcoming the shortcomings of two-dimensional transabdominal and two-dimensional transvaginal ultrasound [11]. VCI-C uses surface transformation to obtain relevant tissue information from adjacent thin layers, and improves the contrast of originally similar tissues or structures in traditional two-dimensional ultrasound to form clearer internal structures and boundaries of tissues and organs [12, 13]. Therefore, VCI-C technology can improve the contrast of ultrasound images and reduce noise interference. Gunbey et al. successfully observed the primary fissure of the cerebellar vermis of 173 normal fetuses at 18-26 weeks using VCI-C, measured the upper and lower diameters of the cerebellar vermis and found that they were related to gestational age [14]. In 1983, Martinez-Ten et al. first applied magnetic resonance imaging (MRI) to the diagnosis of fetal malformations [15]. With the development of MRI fast imaging sequence technology, MRI has been widely used to diagnose fetal malformations. MRI has the advantages of good soft tissue resolution, high contrast, wide imaging field, and multi-directional imaging, and is not affected by factors such as maternal obesity, fetal amniotic fluid volume, fetal position and fetal bone [16]. It is known as the "gold standard" for diagnosing fetal head malformation. However, due to the expense of MRI equipment, the high examination cost and long examination time, it is rarely used at present. Also, it is unable to perform real-time imaging on the fetus. The image quality is compromised by fetal movement and fetal heartbeat, and there are contraindications such as claustrophobic syndrome and risk factors such as thermal effect, so it is not a first choice for diagnosis of fetal malformations [17]. However, due to the influence of objective factors such as fetal position, maternal obesity, and skull sound attenuation, the traditional two-dimensional prenatal ultrasound can easily obtain the transverse section of fetal cerebellar vermis, but this section cannot evaluate the overall development of the vermis [18]. It is difficult to obtain the central sagittal section of fetal head necessary for observing fetal cerebellar vermis by traditional two-dimensional ultrasound scanning.

In this study, three-dimensional VCI-C plane was used to quantitatively evaluate the development of fetal cerebellar vermis and posterior cranial fossa lesions. Combined with the advantages of MRI in soft tissue resolution, the morphology of the fetal cerebellar vermis and cerebellar tentorium was observed, and the differences between the images obtained by the two imaging methods were analyzed and compared, so as to explore their diagnostic value and consistency for detection of abnormalities. This research combines VCI-C and MRI to diagnose the lesions of the posterior cranial fossa of the fetus, and makes full use of the 3.0 superconducting magnetic resonance rapid imaging sequence to solve the problem of ultrasound being affected by objective factors such as fetal position, obesity, and amniotic fluid volume. This gives clear morphologic and structural images of the fetal small brain vermis and posterior cranial fossa, improves the diagnostic accuracy, and avoids missed diagnosis and misdiagnosis.

Materials and methods

Study design

This study retrospectively analyzed the imaging data of 100 pregnant women suspected to have abnormal development of fetal cerebellar vermis and posterior cranial fossa in the First Affiliated Hospital of Gannan Medical University from January 2020 to February 2022. The study was approved by Ethics Committee of First Affiliated Hospital of Gannan Medical University.

Inclusion criteria

(1) Singleton pregnant women with gestational age of 20-40 w; (2) Pregnant women with no pregnancy complications; (3) Pregnant women with complete data of ultrasonic examination; (4) Pregnant women with neither abnormalities of the central nervous system found by prenatal ultrasound screening and MRI, nor obvious abnormality found in the follow-up after birth.

Exclusion criteria

(1) Pregnant women with images of poor quality and unclear display of median sagittal plane due to fetal movement; (2) Pregnant women with incomplete clinical data.

VCI-C technology

Ge volution three-dimensional color Doppler ultrasound diagnostic instrument was used for detection. The two-dimensional ultrasound probe c1-5-d, with a frequency of 3-5 MHz, was used for routine obstetric ultrasound examination. After measuring the fetal biparietal diameter, head circumference, and cerebellar transverse diameter, the transabdominal three-dimensional volume probe, with a frequency of 4-8 MHz, was used. The three-dimensional VCI-C mode was used to adjust the volume layer thickness to 3 mm, then we scanned the fetal head in a quiet state to display the transverse section of the cerebellum. After obtaining the best plane, the three-dimensional volume scan was performed. We adjusted the sampling volume, including the whole head of the fetus, instructed the pregnant woman to hold her breath to avoid fetal movement, and then started automatic volume scanning (1-2 s). After obtaining the three-dimensional volume data of the fetal brain, we conducted image processing. To be specific, we called out the three-dimensional data and displayed the three orthogonal sectional images of A, B, and C3 that were perpendicular to each other, set the central indicator point of plan A and B between the two cerebellar hemispheres, rotated the image to plane A, which was the transverse section of the cerebellum, and plane B, which was the coronal section of the cerebellum. At this time, plane C displayed the sagittal section through the cerebellar vermis. We selected VCI mode, adjusted the image to clearly display the corpus callosum, transparent septum and cerebellar vermis, and observed the morphology of the cerebellar vermis, fine structures such as the primary fissure, secondary fissure and each lobule, the morphology of the fourth ventricle, and the relationship between the vermis and adjacent tissues such as brainstem and tentorium cerebellum. The superior inferior diameter (CC), anterior posterior diameter (AP), area (MSA), and circumference of cerebellar vermis were measured (C).

MRI examination

Philips 1.5T superconducting magnetic resonance scanner, body coil, layer thickness 4 mil, layer spacing 4 mm, matrix 256 × 256, sense technology, turbo field echo for T1WI and high-resolution sssh.tse sequence for T2WI were adopted. The same pregnant woman underwent MRI examination of fetal head during pregnancy, and the interval between MRI examination and three-dimensional VCI-C was within one week. The pregnant woman was in a supine position, with advanced feet, and was scanned while holding her breath. The sagittal and cross-sectional scans of fetal cerebellar vermis were routinely performed, and the images were collected and saved. We selected the median sagittal section of fetal cerebellar vermis on T2 weighted images, and observed the morphology, primary fissure, and secondary fissure of cerebellar vermis after enlarging the images. On the enlarged fetal j6d, the BVA (the angle formed by the dorsal tangent of the brain stem and the ventral tangent of the cerebellar vermis) and BTA (the angle formed by the dorsal tangent of the brain stem and the tentorial tangent) were measured on the median sagittal plane of the cerebral vermis.

Evaluation indicators

(1) Height and anteroposterior diameter of fetal cerebellar vermis: On the median sagittal image of fetal cerebellar vermis, the maximum distance between the head and tail of fetal cerebellar vermis measured in the parallel direction

Table 1. Comparison of baseline data between the two groups ($\overline{x}$ ± s)

	VCI-C combined with MRI group (n = 58)	MRI group (n = 42)	t/χ^2	P
Age	31.21±3.86	31.73±3.33	1.658	0.127
BMI before pregnancy	24.74±2.67	24.35±3.41	1.178	0.278
Parity			2.198	0.148
Primipara	40 (69.0%)	28 (66.7%)		
Parturient women	18 (31.0%)	14 (33.3%)		
fetuses with cerebellar vermis dysplasia	13 (22.4%)	4 (9.5%)	8.21	0.012
fetuses with arachnoid cyst	10 (17.2%)	6 (14.3%)	3.32	0.048
fetuses with Blake cyst	11 (19.0%)	8 (19.0%)	4.87	0.032
fetuses with Dandy Walker malformation	9 (15.5%)	4 (9.5%)	7.98	0.036

Note: VCI-C: Volume Contrast Imaging C; MRI: Magnetic Resonance Imaging; BMI: Body Mass Index.

of brain stem is the height of cerebellar vermis. The maximum anteroposterior diameter of fetal cerebellar vermis was measured at the top of the fourth ventricle. (2) Area of fetal cerebellar vermis: The contour of fetal cerebellar vermis was manually drawn on the median sagittal section image of fetal cerebellar vermis, which was processed by us and MRI matching correlation analysis software. (3) BVA and BTA: The included angle between the dorsal tangent of brainstem and the ventral tangent of cerebellar vermis and the angle between the dorsal tangent of brainstem and the tangent of tentorium cerebelli were measured.

Statistical processing

SPSS22.0 statistical software was used for analysis. The measured data were tested to be in accordance with the normal distribution, expressed by mean ± standard deviation ($\overline{X}$ ± SD). The independent sample t-test was used for comparison between the two groups. Counted data were expressed as number of cases (percentage) [n (%)]. The height, anteroposterior diameter, area, BVA, and BTA of fetal cerebellar vermis measured on three-dimensional VCI-C and MRI images were compared. A difference was significant at $P < 0.05$.

Results

Comparison of baseline data between the two groups

This study showed no difference in age, body mass index before pregnancy or parity between groups (P > 0.05). The diagnoses of fetuses with cerebellar vermis dysplasia, arachnoid cyst, Blake cyst, and Dandy Walker malformation between the two groups had a significant difference (P < 0.05) (**Table 1**).

Consistency analysis of VCI-C and MRI in displaying the morphology, primary fissure, and secondary fissure of the fetal cerebellar vermis of in fetuses with greater occipital cisterna

As shown in **Figure 1**, VCI-C plane was highly consistent with MRI in displaying the morphology, primary fissure, and secondary fissure of fetal cerebellar vermis in fetuses of greater occipital cisterna (Kappa = 0.91). Moreover, the median sagittal plane showed that the vermis was full, and the top of the fourth ventricle was depressed (**Figure 1A**).

Consistency analysis of VCI-C and MRI in displaying the morphology, primary fissure, and secondary fissure in fetuses with cerebellar vermis dysplasia

VCI-C plane was consistent with MRI in displaying the morphology, primary fissure, and secondary fissure in fetuses with cerebellar vermis dysplasia (Kappa = 0.83) (**Figure 2**).

Consistency analysis of VCI-C and MRI in displaying the morphology, primary fissure, and secondary fissure in fetuses with arachnoid cyst

In fetuses with arachnoid cyst, there was a high consistency between VCI-C and MRI in displaying the morphology, primary fissure, and secondary fissure (Kappa = 0.88) (**Figure 3**).

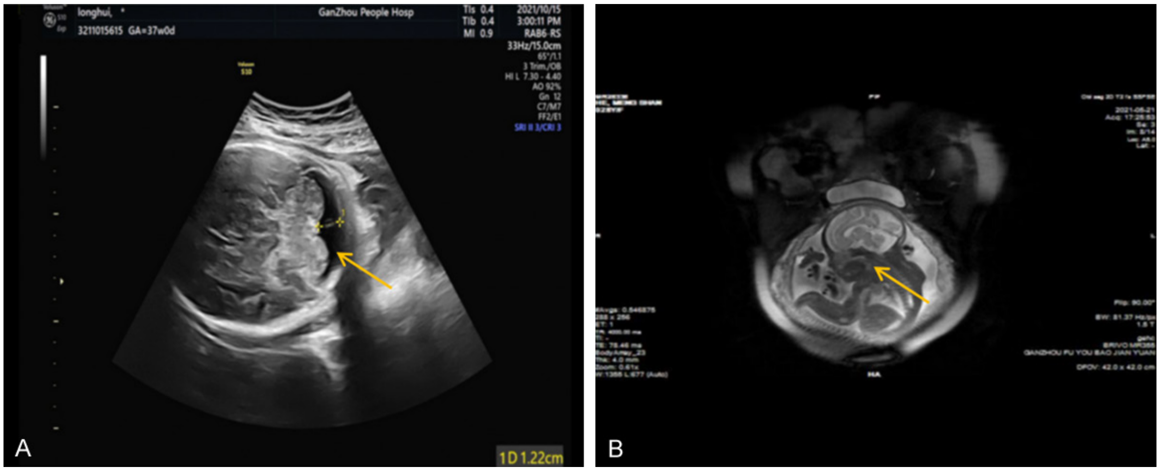

Figure 1. Consistency analysis of VCI-C and MRI in measuring BVA and BTA of fetal cerebellar vermis in fetuses of greater occipital cisterna. A: VCI-C; B: MRI. VCI-C: Volume Contrast Imaging C; MRI: Magnetic Resonance Imaging; BVA: angle between brain stem and cerebellar vermis; BTA: angle between brain stem and cerebellar tentorium.

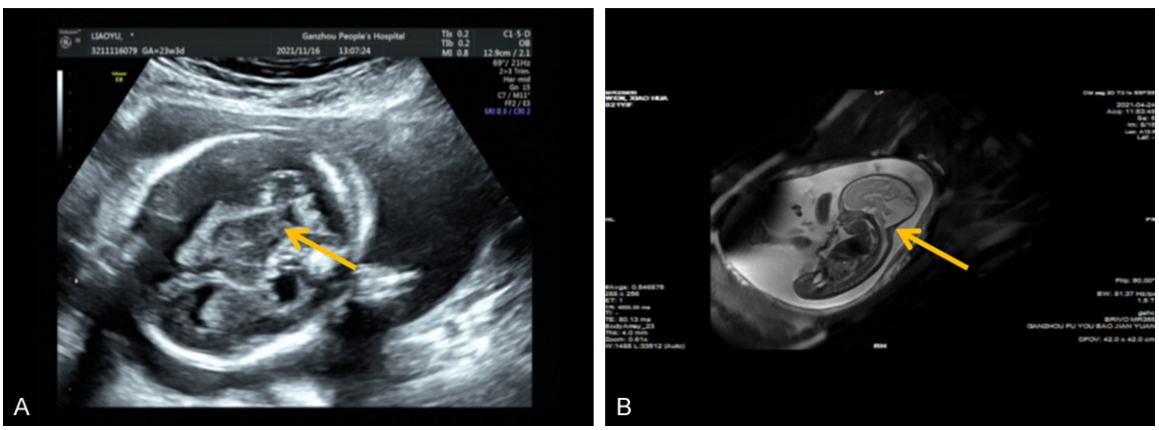

Figure 2. Consistency analysis of VCI-C and MRI in displaying the morphology, primary fissure, and secondary fissure in fetuses with cerebellar vermis dysplasia. A: VCI-C; B: MRI. VCI-C: Volume Contrast Imaging C; MRI: Magnetic Resonance Imaging.

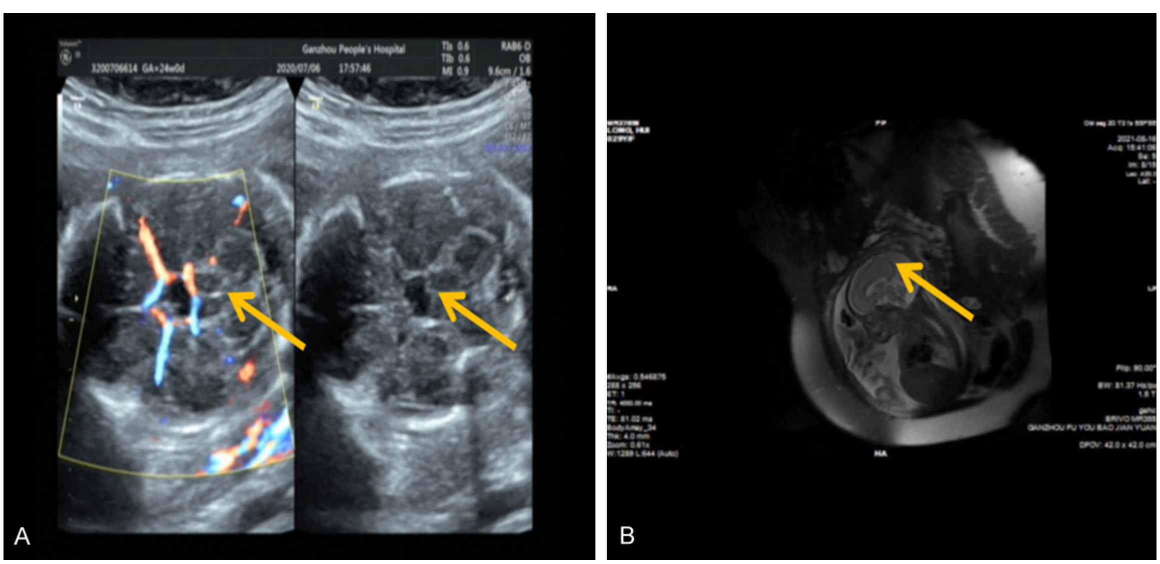

Figure 3. Consistency analysis of VCI-C and MRI in displaying the morphology, primary fissure, and secondary fissure in fetuses with arachnoid cyst. A: VCI-C; B: MRI. VCI-C: Volume Contrast Imaging C; MRI: Magnetic Resonance Imaging.

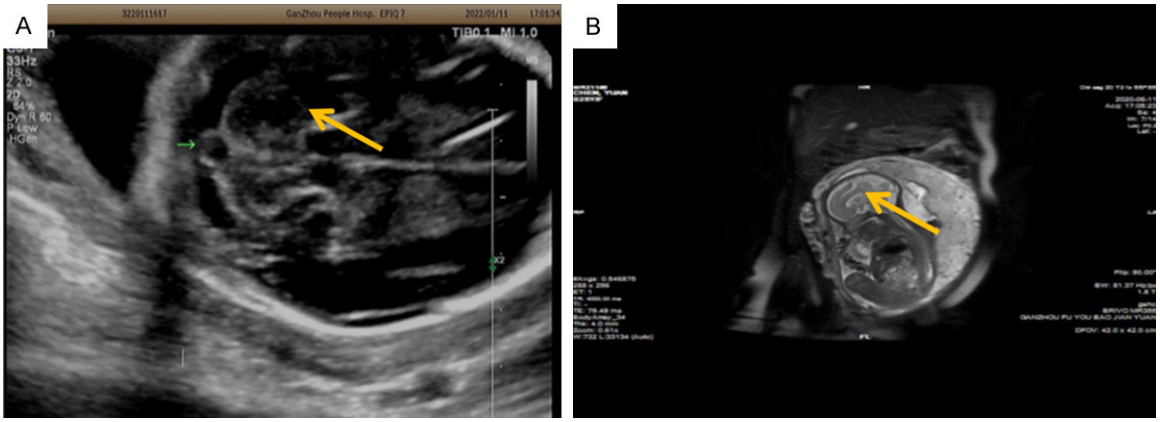

Figure 4. Consistency analysis of VCI-C and MRI in displaying the morphology, primary fissure, and secondary fissure in fetuses with Blake cyst. A: VCI-C; B: MRI. VCI-C: Volume Contrast Imaging C; MRI: Magnetic Resonance Imaging.

Consistency analysis of VCI-C and MRI in displaying the morphology, primary fissure, and secondary fissure in fetuses with Blake cyst

In the fetuses with Blake cyst, the VCI-C plane was consistent with MRI in displaying the morphology, primary fissure, and secondary fissure (Kappa = 0.78) (**Figure 4**). As shown in **Figure 4A**, the median sagittal plane showed that the vermis was full in its shape, and the top of the fourth ventricle was flat and shallow, and connected with the posterior fossa cistern after expansion.

Consistency analysis of VCI-C and MRI in displaying the morphology, primary fissure, and secondary fissure in fetuses with Dandy Walker malformation

In fetuses with Dandy Walker malformation, there was a high consistency between VCI-C and MRI in displaying the morphology, primary fissure, and secondary fissure (Kappa = 0.91) (**Figure 5**). **Figure 5A** in the median sagittal plane shows that the area of the vermis was significantly reduced, and the morphologic structure was abnormal. The primary fissure and secondary fissure are not shown. After the expansion of the fourth ventricle, the posterior fossa pool was connected.

Comparison of BVA and BTA of VCI-C and MRI in various posterior fossa malformations

In various posterior fossa malformations, there was a significant difference in the BVA between VCI-C and MRI images ($P < 0.05$). Furthermore, there was a significant difference in the BVA between VCI-C and MRI images in fetuses with Dandy Walker malformation, Blake cyst, and arachnoid cyst ($P < 0.05$) (**Table 2**).

Receiver operating characteristic (ROC) curve analysis

ROC curve results showed that the area under the curve of VCI-C combined with MRI in the diagnosis of fetal cerebellar vermis and posterior cranial fossa was 0.793982 [(95% CI, 0.690-0.866), $P < 0.001$] (**Figure 6**).

Discussion

The cerebellar vermis connects the cerebellar hemispheres on both sides and is located in the middle of the cerebellum. It is narrow and curly in shape. It begins to develop from the midline of the cerebellar hemispheres at the 9th week of pregnancy, and can form a complete vermis at the 15th week [19, 20]. However, clinical observation found that the cerebellar vermis may stay in an open state at the 18th week of pregnancy, so it is still impossible to diagnose abnormal development of the vermis before the 18th week of pregnancy. The main feature of vermis malformation is its absence. Therefore, measures of the vermis have value in evaluating lesions of the posterior cranial fossa. Three dimensional ultrasonic VCI C-plane imaging belong to the space composite imaging technology. This collects and processes the

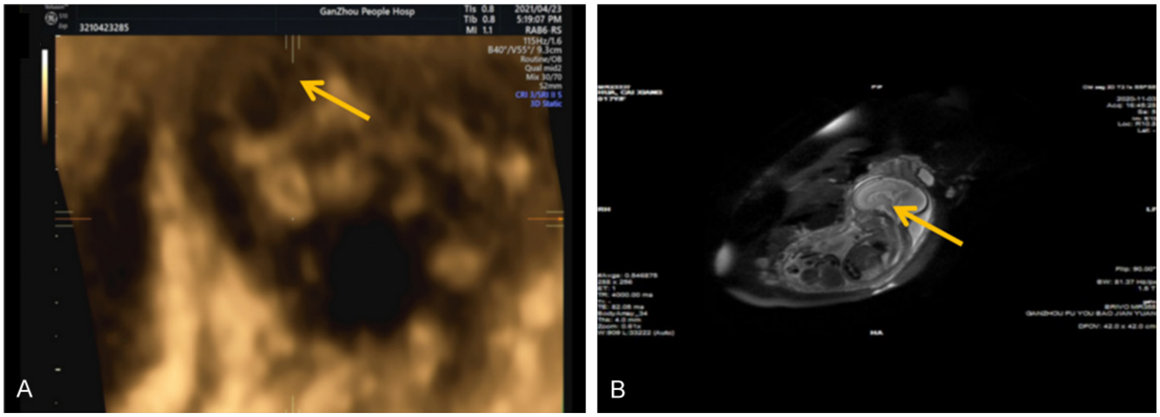

Figure 5. Consistency analysis of VCI-C and MRI in displaying the morphology, primary fissure, and secondary fissure in fetuses with Dandy Walker malformation. A: VCI-C; B: MRI. VCI-C: Volume Contrast Imaging C; MRI: Magnetic Resonance Imaging.

Table 2. Comparison of BVA and BTA of VCI-C and MRI in various posterior fossa malformations ($\bar{x} \pm s$)

Index	time	Fetal cerebellar vermis in fetuses of greater occipital cisterna	Cerebellar vermis dysplasia	Arachnoid cyst	Blake cyst	Dandy Walker malformation
BVA	VCI-C	3.31±1.27	3.43±0.25	23.13±1.25	13.23±1.25	83.73±0.25
	MRI	2.28±1.16	2.71±0.21	21.11±1.21	9.21±1.21	81.71±0.21
	t	4.216	3.214	5.214	4.224	3.214
	P	0.047	0.048	0.036	0.048	0.038
BTA	VCI-C	23.31±1.27	49.22±1.25	35.22±1.25	68.22±0.25	88.42±0.25
	MRI	26.80±1.34	47.93±1.21	21.93±1.21	57.93±1.21	70.93±0.21
	t	8.728	6.146	4.146	6.146	3.146
	P	0.061	0.083	0.033	0.043	0.043

Note: VCI-C: Volume Contrast Imaging C; MRI: Magnetic Resonance Imaging; BVA: angle between brain stem and cerebellar vermis; BTA: angle between brain stem and cerebellar tentorium.

volume data in multiple sections, so that the deeper pixels are brought to positions where the surface gray value information is missing and gaps are left. Filling the gaps makes the speckled part of the image smooth, the image clearer, and the display of the cerebellar vermis clearer. Compared to two-dimensional ultrasound and MRI, the primary fissure and secondary fissure of the cerebellar vermis can be displayed earlier [20, 21].

Compared to traditional two-dimensional ultrasound, the three-dimensional ultrasound VCI-C provides a homogeneous, noise reduced, and contrast enhanced image that can easily obtain a median sagittal section of the fetal cerebellar vermis [22]. As an image post-processing technology, it can greatly reduce examination time, and reduce irradiation time from the ultrasound to the fetus and pregnant women, with convenient operation and high reliability [23]. Compared to MRI, three-dimensional ultrasound VCI-C has the advantages of low price, convenience, time saving, non-radiation, continuous dynamic and repeated scanning, and can overcome the influence of maternal respiratory movement and fetal movement on the image quality of MRI. There are no contraindications for its use with fetal posterior fossa lesions.

The results of this study showed that VCI-C and MRI had the highest consistency in showing whether fetal JLD and cerebral vermis were normal, and good consistency in showing whether the primary fissure was clear. However, the consistency in showing whether the secondary fissure was clear was only acceptable. This may

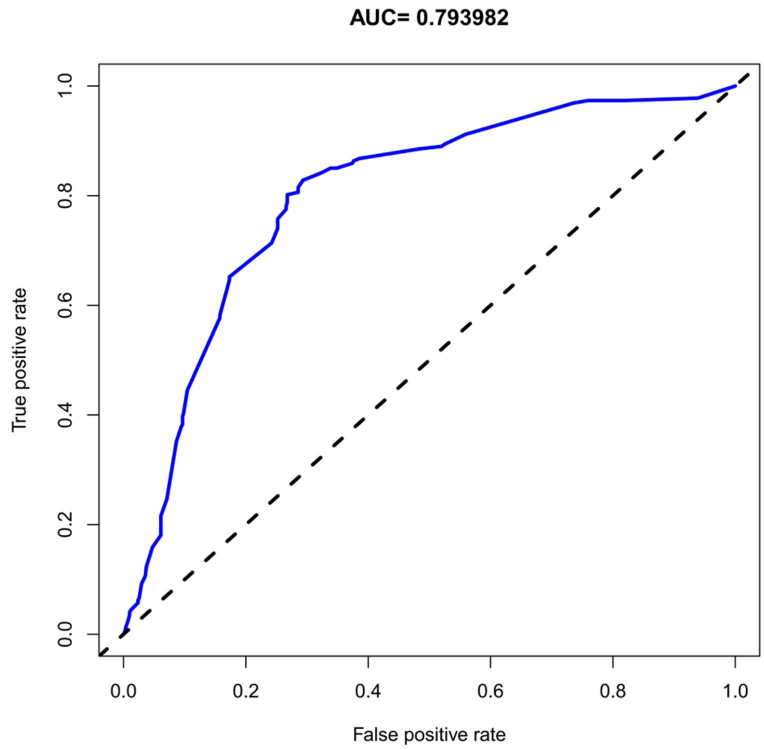

Figure 6. ROC curve analysis of VCI-C combined with MRI in the diagnosis of the fetal cerebellar vermis and the posterior cranial fossa. AUC: Area Under The Curve; ROC: Receiver Operating Characteristic; VCI-C: Volume Contrast Imaging C; MRI: Magnetic Resonance Imaging.

be because the VCI-C and MRI are not clear enough in showing the fine structures of the vermis such as the secondary fissure in some fetuses. This might bias the diagnosis, depending on the diagnostic tendencies of the radiographer. Garcia-Posada et al. [24] used VCI-C to measure the cerebellar vermis and detected the primary fissure. All the subjects were fetuses in mid-pregnancy. Comparing the three-dimensional ultrasound images of the fetal cerebellar vermis obtained by VCI-C, it was found that the images obtained from the late pregnancy fetus were not as clear as those obtained from the middle pregnancy fetus, and the clarity of fine structures such as the secondary fissure was poor. The reason for the reduction in image quality may be related to the thickness of the abdominal wall of the pregnant woman, uterine leiomyoma, poor position of the fetus, or reduced amniotic fluid. The image of fetal cerebellar vermis obtained by MRI with a magnetic field strength of 3.0T was clearer. However, considering the risk factors such as thermal effect of MRI, 1.5 tmri is still used in clinical practice.

The results of this study show that VCI-C and MRI were consistent in measuring BVA and BTA on the median sagittal plane of cerebellar vermis of fetuses with posterior fossa malformation, and the measured range of BVA and BTA was close to that reported by Tilea et al. [25]. They reported that BVA and BTA of various posterior cranial fossa malformations were measured due to different degrees of rotation of cerebellar vermis or cerebellar tentorium. This rule is conducive to the diagnosis and differential diagnosis of various fetal posterior cranial fossa malformations in clinical work [26]. Due to the small number of cases collected in this paper, our data may not accurately reflect the BVA and BTA of various posterior fossa malformations in the Chinese population. Therefore, in the future work, we will collect more cases to further measure BVA and BTA, so as to find the degree suitable for Chinese people, and provide a quantitative basis for diagnosis and differential diagnosis of various posterior cranial fossa malformations.

In sum, VCI-C plane can clearly display the median sagittal section of the fetal cerebellar vermis in a normal control group and a cerebellar vermis dysplasia group, and can accurately evaluate the development of the vermis. It is comparable to MRI for observing vermis development. Three-dimensional ultrasound has the advantages of low price, convenience, time saving, no trauma, no radiation, continuous dynamic observation of fetal posterior fossa structure, and good reproducibility. It can also overcome image artifacts caused by the patient's respiratory movement and fetal movement. Therefore, VCI-C can be widely used in the clinic as a routine means for prenatal diagnosis, identification of fetal cerebellar vermis dysplasia. and regular reexamination of suspected fetuses suggested by MRI.

Disclosure of conflict of interest

None.

Address correspondence to: Huan Lu, Department of Ultrasound Medicine, The First Affiliated Hospital of Gannan Medical University, Qingnian Road, Zhanggong District, Ganzhou 341000, Jiangxi, China. Tel: +86-0797-8266045; E-mail: luhuan-6356@163.com

References

[1] Kose S, Altunyurt S and Keskinoglu P. A prospective study on fetal posterior cranial fossa assessment for early detection of open spina bifida at 11-13 weeks. Congenit Anom (Kyoto) 2018; 58: 4-9.
[2] Eric Ozdemir M, Demirci O, Ayvaci Tasan H, Ohanoglu K and Akalin M. The importance of first trimester screening of cranial posterior fossa in predicting posterior fossa malformations which may be identified in the following weeks of gestation. J Clin Ultrasound 2021; 49: 958-962.
[3] Volpe P, De Robertis V, Volpe G, Boito S, Fanelli T, Olivieri C, Votino C and Persico N. Position of the choroid plexus of the fourth ventricle in first- and second-trimester fetuses: a novel approach to early diagnosis of cystic posterior fossa anomalies. Ultrasound Obstet Gynecol 2021; 58: 568-575.
[4] Paladini D, Donarini G, Parodi S, Volpe G, Sglavo G and Fulcheri E. Hindbrain morphometry and choroid plexus position in differential diagnosis of posterior fossa cystic malformations. Ultrasound Obstet Gynecol 2019; 54: 207-214.
[5] Nagaraj UD, Kline-Fath BM, Horn PS and Venkatesan C. Evaluation of posterior fossa biometric measurements on fetal MRI in the evaluation of Dandy-Walker continuum. AJNR Am J Neuroradiol 2021; 42: 1716-1721.
[6] Aertsen M, Verduyckt J, De Keyzer F, Vercauteren T, Van Calenbergh F, De Catte L, Dymarkowski S, Demaerel P and Deprest J. Reliability of MR imaging-based posterior fossa and brain stem measurements in open spinal dysraphism in the era of fetal surgery. AJNR Am J Neuroradiol 2019; 40: 191-198.
[7] Mckinnon K, Kendall GS, Tann CJ, Dyet L, Sokolska M, Baruteau KP, Marlow N, Robertson NJ, Peebles D and Srinivasan L. Biometric assessments of the posterior fossa by fetal MRI: a systematic review. Prenat Diagn 2021; 41: 258-270.
[8] Sun L, Guo C, Yao L, Zhang T, Wang J, Wang L, Liu Y, Wang K, Wang L and Wu Q. Quantitative diagnostic advantages of three-dimensional ultrasound volume imaging for fetal posterior fossa anomalies: preliminary establishment of a prediction model. Prenat Diagn 2019; 39: 1086-1095.
[9] Dovjak GO, Diogo MC, Brugger PC, Gruber GM, Weber M, Glatter S, Seidl R, Bettelheim D, Prayer D and Kasprian GJ. Quantitative fetal magnetic resonance imaging assessment of cystic posterior fossa malformations. Ultrasound Obstet Gynecol 2020; 56: 78-85.
[10] Chapman T, Menashe SJ, Zare M, Alessio AM and Ishak GE. Establishment of normative values for the fetal posterior fossa by magnetic resonance imaging. Prenat Diagn 2018; 38: 1035-1041.
[11] Pier DB, Gholipour A, Afacan O, Velasco-Annis C, Clancy S, Kapur K, Estroff JA and Warfield SK. 3D super-resolution motion-corrected MRI: validation of fetal posterior fossa measurements. J Neuroimaging 2016; 26: 539-544.
[12] Pertl B, Eder S, Stern C and Verheyen S. The fetal posterior fossa on prenatal ultrasound imaging: normal longitudinal development and posterior fossa anomalies. Ultraschall Med 2019; 40: 692-721.
[13] Dall'Asta A, Grisolia G, Volpe N, Schera G, Sorrentino F, Frusca T and Ghi T. Prenatal visualisation of the torcular herophili by means of a Doppler technology highly sensitive for low-velocity flow in the expert assessment of the posterior fossa: a prospective study. BJOG 2021; 128: 347-352.
[14] Gunbey HP, Bilgici MC, Aslan K, Aygün C and Celik H. Ectopic cerebellar tissue of the posterior cranial fossa: diffusion tensor tractography and MR spectroscopy findings. Childs Nerv Syst 2016; 32: 195-198.
[15] Martinez-Ten P, Illescas T, Adiego B, Estevez M, Bermejo C, Wong AE and Sepulveda W. Non-visualization of choroid plexus of fourth ventricle as first-trimester predictor of posterior fossa anomalies and chromosomal defects. Ultrasound Obstet Gynecol 2018; 51: 199-207.
[16] Altmann R, Specht C, Scharnreitner I, Schertler C, Mayer R, Arzt W and Scheier M. Reference ranges for transvaginal examined fossa posterior structures in fetuses from 45 to 84 mm crown-rump length. Gynecol Obstet Invest 2018; 83: 375-380.
[17] Volpe P, Contro E, Fanelli T, Muto B, Pilu G and Gentile M. Appearance of fetal posterior fossa at 11-14 weeks in fetuses with Dandy-Walker malformation or chromosomal anomalies. Ultrasound Obstet Gynecol 2016; 47: 720-725.
[18] Leibovitz Z, Haratz KK, Malinger G, Shapiro I and Pressman C. Fetal posterior fossa dimensions: normal and anomalous development assessed in mid-sagittal cranial plane by three-

dimensional multiplanar sonography. Ultrasound Obstet Gynecol 2014; 43: 147-153.
[19] Altmann R, Scharnreitner I, Scheier T, Mayer R, Arzt W and Scheier M. Sonoembryology of the fetal posterior fossa at 11+3 to 13+6 gestational weeks on three-dimensional transvaginal ultrasound. Prenat Diagn 2016; 36: 731-737.
[20] Chapman T, Mahalingam S, Ishak GE, Nixon JN, Siebert J and Dighe MK. Diagnostic imaging of posterior fossa anomalies in the fetus and neonate: part 2, posterior fossa disorders. Clin Imaging 2015; 39: 167-175.
[21] Milani HJF, Barreto EQS, Ximenes RLDS, Baldo CAR, Araujo Júnior E and Moron AF. Fetal posterior fossa malformations: review of the current knowledge. Radiol Bras 2019; 52: 380-386.
[22] Robinson AJ and Ederies MA. Diagnostic imaging of posterior fossa anomalies in the fetus. Semin Fetal Neonatal Med 2016; 21: 312-320.
[23] Limperopoulos C, Robertson RL Jr, Khwaja OS, Robson CD, Estroff JA, Barnewolt C, Levine D, Morash D, Nemes L, Zaccagnini L and du Plessis AJ. How accurately does current fetal imaging identify posterior fossa anomalies? AJR Am J Roentgenol 2008; 190: 1637-1643.
[24] Garcia-Posada R, Eixarch E, Sanz M, Puerto B, Figueras F and Borrell A. Cisterna magna width at 11-13 weeks in the detection of posterior fossa anomalies. Ultrasound Obstet Gynecol 2013; 41: 515-520.
[25] Tilea B, Delezoide AL, Khung-Savatovski S, Guimiot F, Vuillard E, Oury JF and Garel C. Comparison between magnetic resonance imaging and fetopathology in the evaluation of fetal posterior fossa non-cystic abnormalities. Ultrasound Obstet Gynecol 2007; 29: 651-659.
[26] Gandolfi Colleoni G, Contro E, Carletti A, Ghi T, Campobasso G, Rembouskos G, Volpe G, Pilu G and Volpe P. Prenatal diagnosis and outcome of fetal posterior fossa fluid collections. Ultrasound Obstet Gynecol 2012; 39: 625-631.